# The GALAH Survey: lithium-strong KM dwarfs

M. Žerjal [1]★ M. J. Ireland [1] T. Nordlander,[1,2] J. Lin,[1] S. Buder [3,4]
L. Casagrande [1] K. Čotar,[5] G. De Silva,[6,7] J. Horner,[8] S. Martell [9]
G. Traven,[10] T. Zwitter [5] and the GALAH Collaboration

[1]*Research School of Astronomy & Astrophysics, Australian National University, Canberra, ACT 2611, Australia*
[2]*ARC Centre of Excellence for All Sky Astrophysics in 3 Dimensions (ASTRO 3D)*
[3]*Max Planck Institute for Astronomy (MPIA), Koenigstuhl 17, D-69117 Heidelberg, Germany*
[4]*International Max Planck Research School for Astronomy & Cosmic Physics, the University of Heidelberg, D-69117 Heidelberg, Germany*
[5]*Faculty of Mathematics and Physics, University of Ljubljana, Jadranska 19, 1000 Ljubljana, Slovenia*
[6]*Sydney Institute for Astronomy, School of Physics, A28, The University of Sydney, Sydney, NSW 2006, Australia*
[7]*Australian Astronomical Observatory, 105 Delhi Rd, North Ryde, NSW 2113, Australia*
[8]*Centre for Astrophysics, University of Southern Queensland, Toowoomba, Qld 4350, Australia*
[9]*School of Physics, UNSW, Sydney, NSW 2052, Australia*
[10]*Lund Observatory, Department of Astronomy and Theoretical Physics, Box 43, SE-221 00 Lund, Sweden*

## ABSTRACT

Identifying and characterizing young stars in the Solar neighbourhood is essential to find and describe planets in the early stages of their evolution. This work seeks to identify nearby young stars showing a lithium 6708 Å absorption line in the GALAH survey. A robust, data-driven approach is used to search for corresponding templates in the pool of 434 215 measured dwarf spectra in the survey. It enables a model-free search for best-matching spectral templates for all stars, including M dwarfs with strong molecular absorption bands. 3147 stars have been found to have measurable lithium: 1408 G and 892 K0–K5 dwarfs (EW(Li) > 0.1 Å), 335 K5–K9 (>0.07 Å) and 512 M0–M4 dwarfs (>0.05 Å). Stars with such lithium features are used to investigate the possibility of searching for young stars above the main sequence based merely on their parallaxes and broad-band photometry. The selection of young stars above the main sequence is highly effective for M dwarfs, moderately effective for K dwarfs and ineffective for G dwarfs. Using a combination of the lithium information and the complete 6D kinematics from *Gaia* and GALAH, 305 new candidate moving group members have been found, 123 of which belong to the Scorpius–Centaurus association, 36 to the Pleiades and 25 to the Hyades clusters.

**Key words:** stars: abundances – stars: late-type – stars: pre-main-sequence.

## 1 INTRODUCTION

Over the past decade, a variety of surveys have greatly enhanced our knowledge of planets orbiting other stars. The *Kepler* space telescope (Borucki et al. 2010) carried out the first large census of the exoplanet era, and revealed that planets on short-period orbits are ubiquitous (e.g. Batalha et al. 2013; Mullally et al. 2015), whilst radial velocity surveys have begun to discover the first true Jupiter-analogues around Sun-like stars (e.g. Marcy et al. 2002; Boisse et al. 2012; Wittenmyer et al. 2014, 2016). In the coming years, it is widely anticipated that the number of known planets will increase dramatically, with NASA's Transiting Exoplanet Survey Satellite (TESS; launched in April 2018, Ricker et al. 2015) expected to

deliver thousands of new planets in the next 2 yr. Complementing the results of TESS, the *Gaia* mission may discover as many as 20 000 additional exoplanets by astrometry (Perryman et al. 2014). Indeed the first exoplanet to be both directly imaged (including a spectrum and planet rotational velocity) and to have a measured mass recently had its mass measured using a combination of an early *Gaia* data release and HIPPARCOS (Snellen & Brown 2018).

In order to take full advantage of these recent discoveries, and the plethora of new finds expected as a result of *TESS* and *Gaia*, it is imperative that we understand the basic characteristics of those stars which host them. Such knowledge is critical to our understanding of the formation and evolution of those planets. For example, there appears to be a lack of hot Jupiters around $\lesssim$20 Myr old stars (Rizzuto et al. 2017), hinting that hot Jupiters may not form by disc-driven migration. This tentative result requires age knowledge of a much larger sample of stars, both for detections and null results

★ E-mail: Marusa.Zerjal@anu.edu.au

with TESS. Interpreting the luminosity of astrometrically detected giant planets requires robust age indicators, especially for young stars where planetary system evolution is most rapid and there is a chance of directly detecting thermal emission from giant planets.

The importance of such accurate characterization can be seen from studies of the directly imaged objects orbiting the star HR 8799 (Marois et al. 2008, 2010; Konopacky et al. 2016; Wertz et al. 2017). The precise mass and nature of those planets is highly dependent on the accurate parametrization of the star, the results of which could have a significant impact on the stability of the planets, and the mass of the associated debris discs in that system (e.g. Marshall, Horner & Carter 2010; Baines et al. 2012; Goździewski & Migaszewski 2014; Contro et al. 2016; Götberg et al. 2016). Over the decade since the HR8799 system was discovered, a better understanding of the nature and age of the host star has resulted in greater confidence that the detected objects are truly planetary in nature. The search for young stars near the Sun, especially those younger than 100 Myr, is thus essential to understand planet formation conditions and their early evolution.

During the early stages in their lives, stars tend to not only share the same birthplace but also a common motion with their siblings. Recently, Gagné et al. (2018, hereafter G18) identified 1406 members of 27 young stellar associations and moving groups within 150 pc of the Sun using their kinematics. Ages of these groups, each containing dozens of stars range from 1 to 800 Myr. The Hyades moving group cluster is generally thought to be one of the oldest known moving groups, with an estimated age between 600 and 800 Myr (Perryman et al. 1998), while the age of the HR1614 is estimated to be 2 Gyr (De Silva et al. 2007). With *Gaia* data release 2 (Gaia Collaboration et al. 2018; *Gaia* DR2) including precise proper motions, parallaxes and radial velocities, the quest to find all nearby ($\lesssim 160$ pc) young moving group members down to substellar types has become feasible (e.g. Gagné & Faherty 2018).

However, most moving groups survive only up to a few hundred million years before they gradually dissolve when passing close to nearby stars and giant molecular clouds. Consequently, assuming that multiple star-forming events took place in the Solar neighbourhood not so long ago, there might be numerous field stars showing signs of youth in their spectra. With the arrival of various and complementary big spectroscopic stellar surveys such as *Gaia* RVS (Sartoretti et al. 2018), APOGEE (Majewski et al. 2017), SEGUE I and II (Yanny et al. 2009), SDSS-V (Kollmeier et al. 2017), RAVE (Kunder et al. 2017), LAMOST (Luo et al. 2015), *Gaia*-ESO (Gilmore et al. 2012), and the future FunnelWeb survey (Rains et al. in prep.), 4MOST (de Jong et al. 2012), WEAVE (Driver et al. 2016) and MOONS (Cirasuolo 2016), systematic searches for young field stars on large scales became possible. For example, Žerjal et al. (2017) found 2000 field stars from the RAVE Survey to be younger than 100 Myr based on their Ca II infrared triplet excess emission. Other spectral features of low-mass young stars include H $\alpha$ emission (West et al. 2008; Schmidt et al. 2015) that remains present up to a few billion years (Mamajek & Hillenbrand 2008) and chromospheric emission in Ca II H&K (e.g. Noyes et al. 1984; Mamajek & Hillenbrand 2008; Zhao et al. 2015). For a review, see Soderblom (2010).

To constrain ages of the youngest, often pre-main sequence (PMS) objects in the first few tens of millions of years of their lives, the presence of the lithium 6708 Å absorption line is used (Soderblom 2010). As PMS objects contract towards the zero-age main sequence and their core temperature reaches $\sim 3 \cdot 10^6$ K, [7]Li ignites on a mass-dependent time-scale. Because the mixing time-scale in fully convective PMS stars is short, lithium becomes depleted throughout the star almost immediately (within a few to ten Myr; Jeffries 2014, i.e. <5 per cent of stellar age). The ignition creates a narrow boundary (lithium depletion boundary) in luminosity between lithium depleted stars and those with lower luminosities that still retain their initial lithium abundance (Soderblom et al. 2014). While the technique can be used for groups of stars with the same age, only upper age limits can be estimated for field stars between 20 and 200 Myr.

This work focuses on data from the Galactic Archaeology with HERMES (GALAH[1]) survey, (De Silva et al. 2015; Martell et al. 2017; Buder et al. 2018), an ongoing large-scale stellar spectroscopic survey of the southern sky that currently contains over 800 000 spectra, among which 98 000 are from the *K2* (Wittenmyer et al. 2018) and 45 000 from the TESS programmes with HERMES (Sharma et al. 2018). The GALAH wavelength range also covers a lithium line in the red channel (6478–6737 Å) that is used to search for young nearby field K and M dwarfs.

The GALAH dataset is presented in Section 2. Data analysis and determination of equivalent widths of lithium absorption line is described in Section 3. lithium-strong pre-main sequence stars and the identification of young stars above the main sequence using broad-band photometry and *Gaia* parallaxes alone, utilizing lithium as a test of the procedure, are discussed in Section 4. Conclusions are given in Section 5.

## 2 DATA

GALAH (De Silva et al. 2015) is an ongoing large-scale spectroscopic survey that makes use of the multi-object (392) spectrograph HERMES (Barden et al. 2010) at the 3.9-metre Anglo-Australian Telescope, located at the Siding Spring Observatory, Australia. The high-resolution spectrograph ($R \sim 28\,000$) is composed of four optical channels covering 4713–4903 Å, 5648–5873 Å, 6478–6737 Å, and 7585–7887 Å. All spectra are continuum normalized. The internal database exceeds 800 000 spectra of 600 000 stars collected between 2014 January and 2018 February. The survey is magnitude limited, with most of the stars between $V_{JK} = 12$ and 14. Additionally, targets were selected from coordinate ranges ($|b| > 10°$) and $-80° < \delta < +10°$ to avoid the crowded and extinction-affected Galactic plane and high airmasses, respectively. The median value of signal-to-noise (S/N) per resolution element in the red arm for candidate spectra is 80, with 90 per cent of stars having S/N better than 40. For more details, including stellar parameter and abundance determination in GALAH, see Buder et al. (2018).

For this study, we restrict ourselves to the red arm of the spectrograph to determine the presence of the lithium absorption line in 438 888 dwarfs. The sample was chosen from 800 000 spectra by exclusion of stars with log $g < 3.75$ and $T_{eff} > 7000$ K, where the stellar parameters are taken from GALAH DR2 (Buder et al. 2018). As not all stars have determined and valid atmospheric parameters, absolute *Gaia* G magnitude (G<2) and BP–RP < 0.5 were used to additionally vet the data. The rest of the stars from the internal database with available radial velocities were kept in the candidate list.

A list of peculiar spectra in GALAH – spectra with features like emission lines, broad TiO bands etc., including spectra affected by technical issues – has been prepared with the t-SNE classification technique (Traven et al. 2017). As the pipelines being used to

---

[1]https://galah-survey.org/
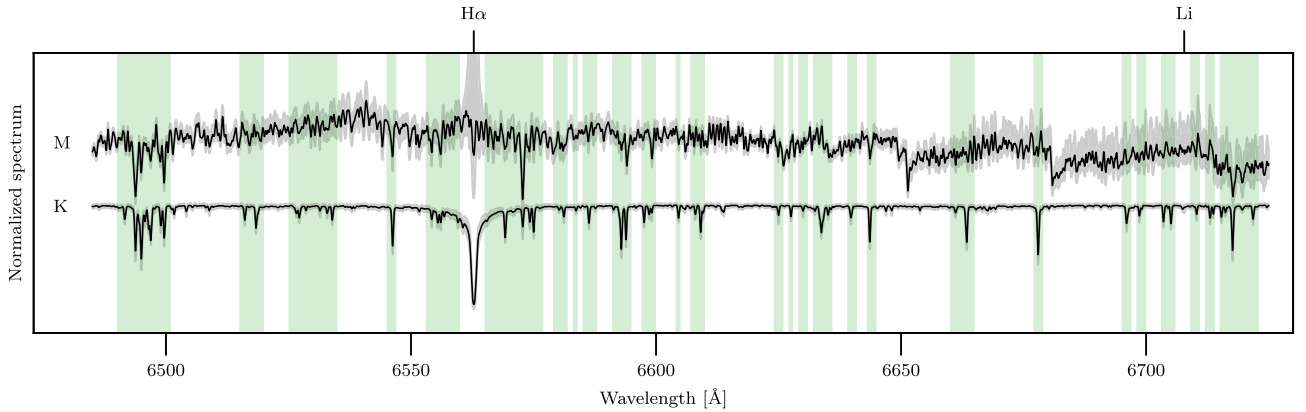
**Figure 1.** The averaged early K and early M spectra in GALAH with deviations (grey areas) due to parameter variations. M dwarfs often show strong H $\alpha$ emission and higher variation of pseudo-continuum above 6650 Å among the sample. Wavelength regions used in the nearest neighbour search are shown by the green bands.
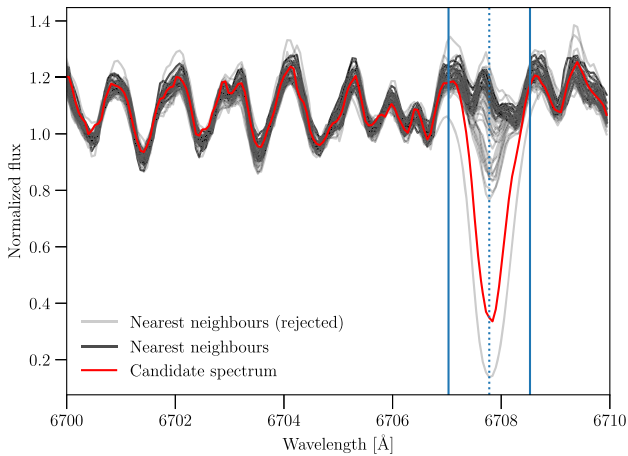


**Figure 2.** An example of a candidate spectrum of an early M dwarf and its nearest neighbours. All spectra are normalized using the same algorithms for all stellar types. Only neighbours with the highest central flux values (at 6708 Å) were kept, the rest were rejected to remove objects with strong lithium. Equivalent width is determined within solid blue lines while dashed line is centred at the Li line.

analyse GALAH data are in some cases not able to treat such spectra, objects from the peculiar list have been excluded from further consideration in the main GALAH survey. However, 5132 very cool stars in this work (mostly M dwarfs) have been selected manually from the list of peculiars with the help of the t-SNE projection and added to the list of lithium-strong candidates. The vetting of the spectra has been done by eye as missing radial velocities for these spectra made the t-SNE projection less efficient. Binary stars have not been treated separately. The fraction of spectra with other types of peculiarity in the sample used in this paper is about 5 per cent.

Radial velocities for the manually selected subsample of 3519 cool peculiars have been determined with cross-correlation using the same pipeline as for the main GALAH survey. The synthetic library AMBRE (de Laverny et al. 2012) has been expanded with inclusion of additional cool templates (3500, 3700, and 3900 K). Metallicity and surface gravity were fixed for all templates (0 and 4.5 dex, respectively). For more details, see Kos et al. (2017). In total, 434 215 spectra of 400 302 unique objects are used in this work. The sample consists of three different subsets: 350 901

GALAH, 62 551 *K2* and 28 955 TESS spectra from the HERMES programs.

## 3 LITHIUM-STRONG DWARFS

The main goal of the GALAH survey is to address the chemical abundances of the stars in the Milky Way galaxy (De Silva et al. 2015). Lithium abundances have been determined for the majority of the stars in the GALAH database. However, due to difficulties in modelling M dwarfs with strong TiO bands and a subsequent lack of a reliable training set, lithium data is unavailable below 4000 K. For this work, we are hence using an independent estimate of the equivalent widths of the lithium line for low-mass stars. The same method is used for both K and M dwarfs to provide consistent measurements across the entire parameter space. A data-driven and model-free approach to obtain equivalent widths from the residual spectra (template minus candidate) is exploited to produce robust and reliable values.

### 3.1 Templates

The estimation of atmospheric parameters in cool stars is complicated. Because the use of synthetic templates is thus not feasible, an alternative 'model free' approach is needed to find observed templates. Because GALAH is a large survey with 800 000 spectra (with about two-thirds being spectra of dwarfs), it is straightforward to take advantage of data-driven and stellar parameter free methods to search for templates among the observed spectra for all types of stars from the hottest to the coolest parts of the Hertzsprung–Russell diagram.

In order to find best-matching observed template spectra for every candidate star, a nearest neighbour search (utilizing KDTree; Pedregosa et al. 2011) among normalized fluxes was performed in a database of 434 215 candidate spectra. Neighbours were searched among candidate spectra themselves.

All GALAH spectra are shifted to the rest frame and interpolated to match the same equidistant wavelength bins ($\Delta\lambda = 0.06$ Å in the red arm). All of them are continuum normalized using the same procedure, and the assumption is that similar stars have similar continuum values, including the depth of the continuum-dominating molecular bands of the coolest stars. 27 wavelength segments of the red arm, that covers the lithium line (Fig. 1), were used in the nearest
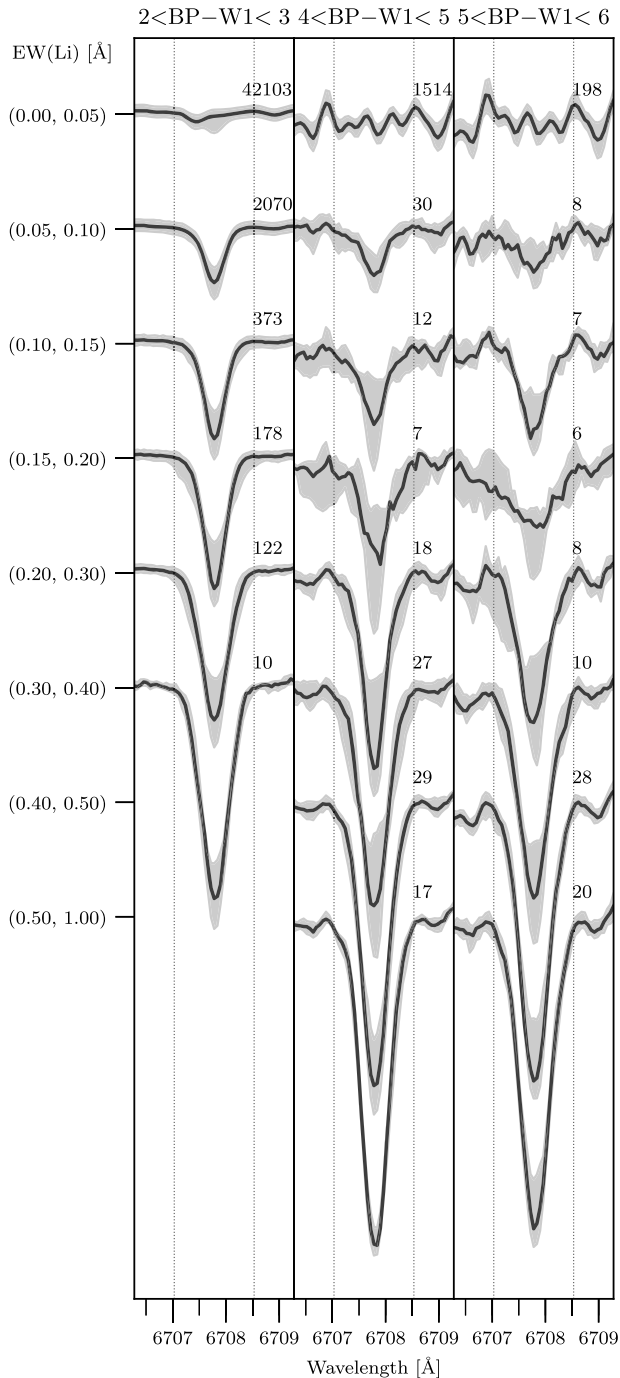
**Figure 3.** Median spectra for BP–*W*1 and EW(Li) bins with 1σ deviations. Spectra with S/N < 40 are excluded. The number of spectra averaged in each bin is given on the right hand side above each median spectrum.

neighbour search. These regions were chosen around the strongest lines with most information, but excluded the lithium and H α line to enable the search for stars with identical spectra but no signs of youth in these two regions.

100 nearest neighbours have been determined for each candidate star. The differences between the colours of candidate spectra and their nearest neighbours are rather small. For the first 50 nearest neighbours, the majority of stars are within (−0.32, +0.14;

corresponding to approximately −100, +50 K) from the star in BP–*W*1 colour.

### 3.2 Equivalent widths

The equivalent width of each lithium line is determined from a selected set of residual spectra. Each candidate spectrum is subtracted from each of its nearest neighbours to determine residual spectra. The procedure is illustrated in Fig. 2. It has two iterations. The steps of the first iteration are:

(i) Find suitable neighbours.

(ii) Correct continuum slope of the candidate spectrum to match its neighbours.

(iii) Add photon noise to the neighbours to match the S/N of the candidate spectrum. Subtract candidate spectrum from its neighbours to get residual spectra.

(iv) Shift residual spectra in flux so that their median outside lithium line is zero.

(v) Find equivalent widths for all residual spectra.

(vi) Determine EW(Li) and uncertainties.

In step (i), a candidate's first 100 nearest neighbours are investigated. Those with S/N ratio less than 40 are rejected. Then, in order to find lithium-weak stars, neighbours are ordered with respect to their flux in the centre of the lithium line. Only those between the 66th and 95th percentile are kept in the pool. A typical number of accepted neighbours is 35 (with an imposed hard upper limit of 50) and they are assumed to represent continuum within the lithium range. From this point on, only wavelengths between 6690 and 6710 Å around the lithium line itself are taken into consideration.

Continuum normalization, especially in the case of very cool stars with wavy pseudo-continuum levels, is sometimes not sufficient at the edges. For this reason, the slope of the candidate is corrected to make sure it overlaps with its nearest neighbours in step (ii). Slope mismatches occur only at the edge and does not affect the nearest neighbour search significantly.

The candidate spectrum is subtracted from each nearest neighbour in step (iii). Residual spectra are shifted along the *y*-axis to match a zero median flux value outside the lithium line [step (iv)]. Equivalent widths are determined for each (*n*th) residual spectrum [step (v)] as

$$\mathrm{EW(Li)}_n = \sum_{i=0}^{N} r_i \Delta\lambda, \qquad (1)$$

where $r_i$ is the residual flux at the *i*th pixel and $N = 25$ is number of pixels in the lithium line between $\lambda_{Li}$-0.75 Å and $\lambda_{Li} + 0.75$ Å. Finally, the EW(Li) of the candidate spectrum is given as a median value of the equivalent widths EW(Li)$_n$ [step (vi)].

Uncertainties are reduced with the second iteration. The latter differs from the iteration 1 only in the step (i) where selection of the most lithium-weak neighbours is based on their EW(Li). In particular, only 15 neighbours with EW(Li) closest to 0 are accepted for every candidate spectrum. The typical measured EW(Li) of selected nearest neighbours is $8 \times 10^{-5}$ Å. This value is well below the measurement error and shows that nearest neighbours have no detectable lithium.

The typical uncertainties of EW(Li) are 0.006 Å for FGK and 0.015 Å for M dwarfs. This is only slightly higher than the uncertainties originating from template mismatch and noise (±0.003 Å), determined from 10 different random intervals outside lithium (but
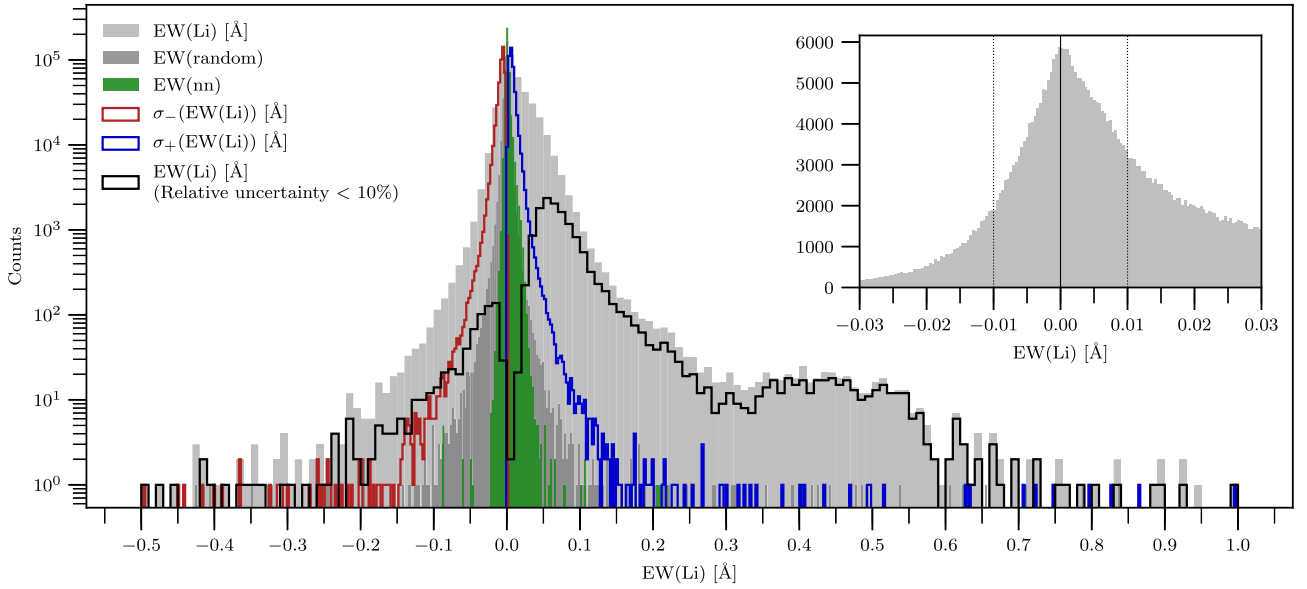
**Figure 4.** Distribution of equivalent width of lithium EW(Li). Most of the stars are lithium weak, but the distribution is bimodal. EW(random) is a measure of fundamental noise and template mismatch uncertainty (0.003 Å). EW(nn) corresponds to lithium-weak templates (nearest neighbours). Note that the *y*-scale is logarithmic. The subplot in a linear scale shows a clear access in positive equivalent width at values as low as 0.01 Å. Bin size in the subplot is refined.
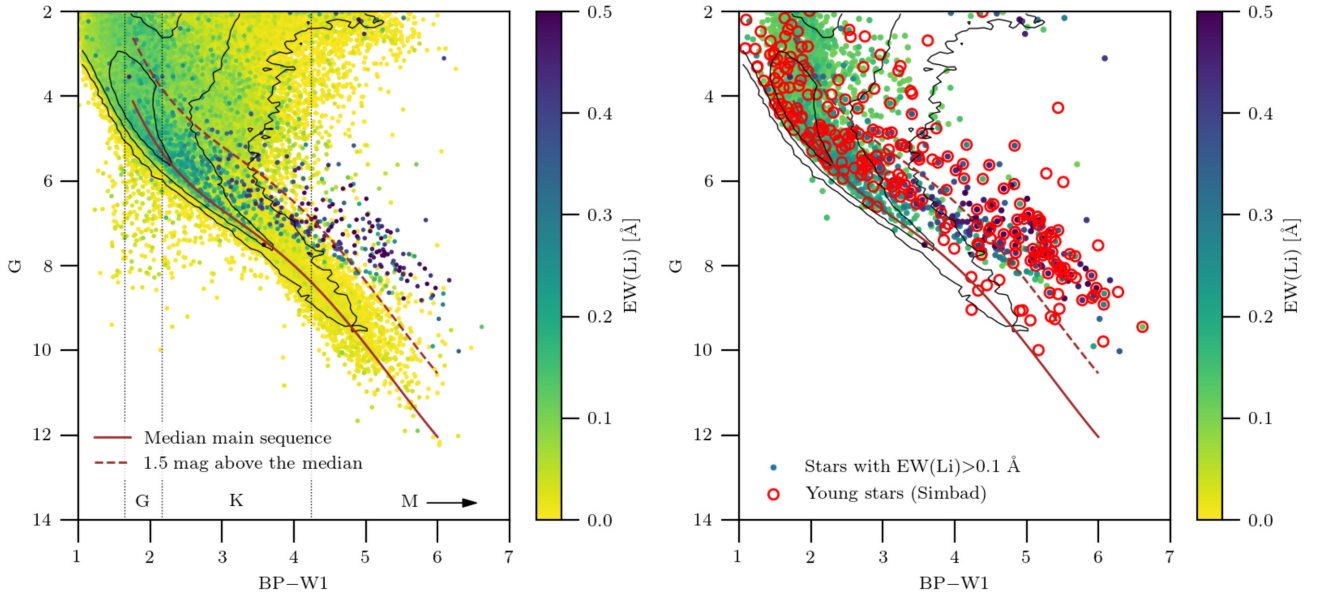


**Figure 5.** Left: Colour–magnitude diagram with absolute G magnitude versus BP–*W*1 for stars with relative parallax errors better than 20 per cent and EW(Li) > 0.037 Å. The majority of lithium-strong stars lie above the main sequence. Number density of stars is designated by the black contours (10, 100, and 1000 stars per 0.1 × 0.1 magnitude bins). Spectral types are marked with vertical lines; BP–*W*1 ≈ 6 corresponds to M4 stars. Right: Stars with EW(Li) > 0.1 Å and stars with young flags in Simbad (red circles; pre-main sequence, X-ray, T Tau, young stellar object). Simbad young stars with missing EW(Li) values (empty red circles) in the plot have either EW(Li) < 0.1 Å or relatively large parallax error.

with same width as the lithium range). Additional uncertainties for the applied method might originate from blending of the CN and Iron I line (6707.441 Å).

The final uncertainties are dominated by the dispersion in EW(Li) of the nearest neighbours. As these templates are also representative of line blends, this error estimation technique includes some systematic errors. Our small error bars are justified by the observed asymmetry of the EW(Li). There is a clear excess in positive equivalent width at values as low as 0.01 Å (Fig. 4). Note

however that our distribution of EW(Li) values has a large tail at low probability to negative values. This is indicative of a some unaccounted for systematic errors in our technique.

Fig. 3 shows an increasing strength of the lithium line in median spectra within EW(Li) bins for four different colour ranges. Although typical EW(Li) uncertainties are small, the lithium line starts to stand out around 0.05 Å (Fig. 3) for stars with BP–*W*1 > 4. The distribution of EW(Li) (Fig. 4), centred at 0.007 Å, is an order of magnitude broader (−0.01, +0.03) Å than uncertainties.
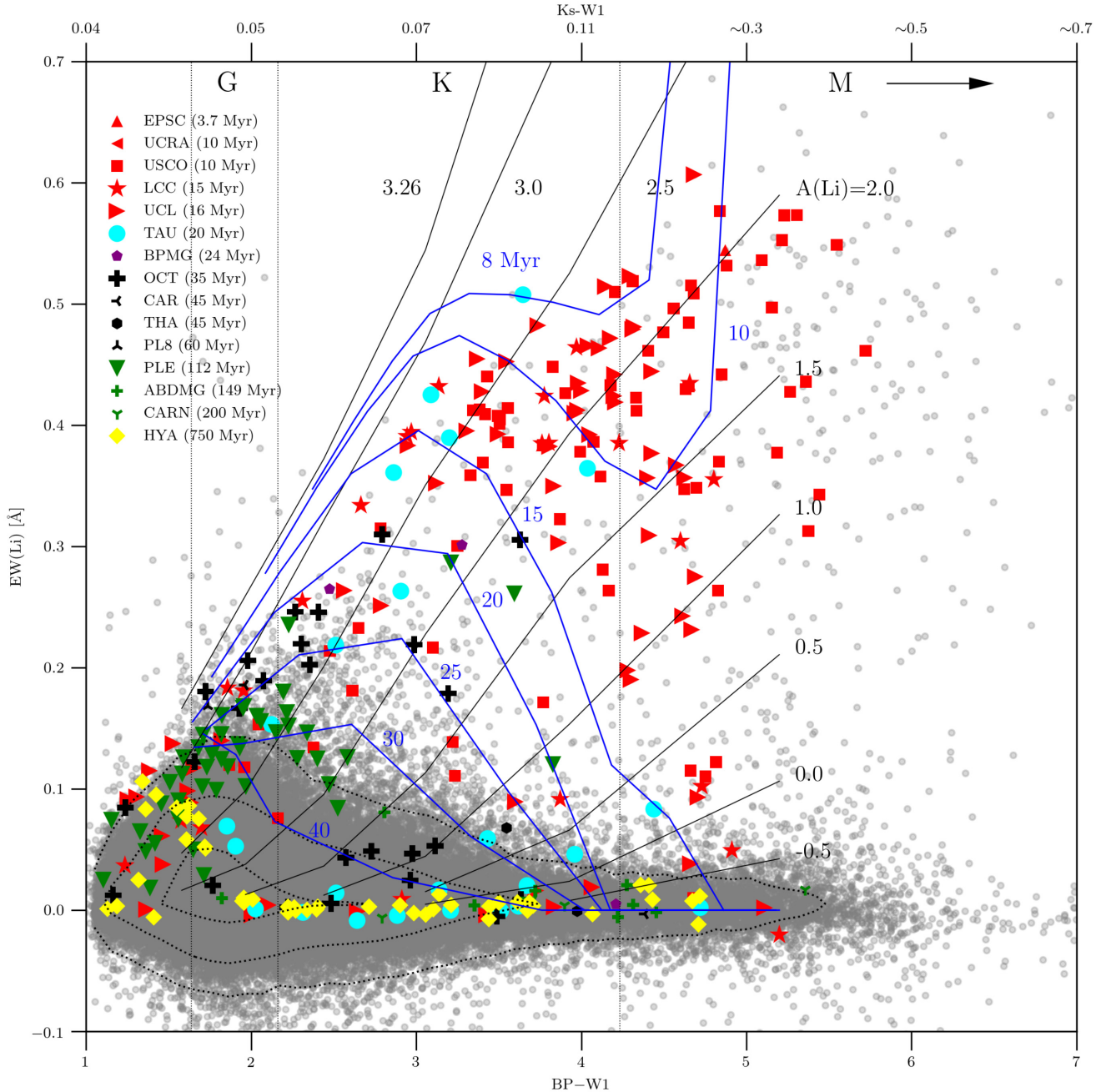
**Figure 6.** The dependence of the measured EW(Li) on the colour for the GALAH stars (grey dots). Contours designate number density (100, 1000, and 10000 stars per 0.1 mag × 0.04 Å). Curves of growth for selected absolute abundances A(Li) for a star with $\log g = 4.45$ and solar metallicity are shown with solid black lines. Isochrones tracking lithium depletion are shown in blue. Bonafide and candidate members of the known moving groups are colour-coded with their age (all these objects are GALAH stars).

## 4 DISCUSSION

The distribution of EW(Li) is shown in Fig. 4. The majority of stars show no lithium absorption line, as expected. The centre of the distribution is at $0.007^{+0.028}_{-0.012}$ Å. However, the distribution does not only seem asymmetrical, with an overabundance of lithium-strong stars, but is also bimodal with the second peak centred at EW(Li)∼0.45 Å and with a width of approximately ±0.2 Å. A few stars are found in the higher range from 0.7 to 1 Å. If the distribution was unimodal and normal with the centre at 0.007 Å and $\sigma = 0.012$ Å [$\sigma$ measured for the left (negative) side of the

distribution], then the number of stars should have fallen below 1 at EW(Li) = 0.1 Å. While the assumption of normal distribution is not entirely true [the number of stars with negative EW(Li) falls to 0 around –0.3 Å], there are 3389 stars with EW(Li) > 0.1 Å, 760 above 0.2 Å, 376 above 0.3 Å, and 102 with EW(Li) > 0.5 Å.

The colour–magnitude diagram (Fig. 5), using *Gaia* DR2 parallaxes (Gaia Collaboration et al. 2018) reveals the nature of stars from the higher EW(Li) peak. Most such stars are M dwarfs with BP–$W1 \gtrsim 4$ which reside above the main sequence – mostly more than 1 mag above the main sequence so they cannot be binaries.

**Table 1.** List of GALAH stars with measured lithium equivalent width. Full version with 434 215 spectra is available online.

| Designation Gaia DR2 | EW(Li) Å | $\sigma$(EW(Li))_ Å | $\sigma$(EW(Li))_+ Å |
|---|---|---|---|
| 6209522875989260032 | 0.021 | 0.002 | 0.007 |
| 5915739214516226688 | 0.056 | 0.005 | 0.006 |
| 6209923617916698240 | 0.038 | 0.008 | 0.005 |
| 6172208513655971072 | 0.033 | 0.002 | 0.005 |
| 6170704519188425600 | 0.012 | 0.007 | 0.010 |

Their EW(Li) is an order of magnitude higher than main sequence stars of the same colour.

As stars with the same temperature would have similar levels of blending and pseudo-continuum depression, it can be concluded that these effects are negligible in this work. Equivalent width is thus a robust measure for the strength of the lithium absorption line for the purpose of discovering young stars. Table 1 lists measured EW(Li) and uncertainties for all 434 215 stars from this work.

For a reference, `astroquery` (Ginsburg et al. 2018) was used to cross-match GALAH with the Simbad catalogue using 2MASS identifiers. Objects marked as young (e.g. 'T Tau' – T Tau-like object, 'pr' – pre-main sequence star, 'Y∗O' – young stellar object, and candidates) show a large overlap with the lithium-strong sequence in Fig. 5 (right).

At a given abundance, the line strength increases with increasing colour (tracing a decreasing effective temperature) as shown in Fig. 6. This is mainly due to the population of the ground state increasing caused by a decreasing ionization fraction. We overplot there indicative non-LTE equivalent widths from Pavlenko & Magazzu (1996), computed for solar metallicity and shown here for $\log g = 4.5$ over a broad range of temperatures and lithium abundances. While these calculations use outdated model atmospheres and neglect transitions due to collisions with neutral hydrogen atoms, they are to our knowledge the only available non-LTE calculations applicable to the range of FGKM-dwarfs analysed here. More recent work on FGK type stars taking into account accurate transition rates (e.g. Lind, Asplund & Barklem 2009) generally predicts larger equivalent widths, with differences at most 20 per cent for the relevant parameter space. Additionally, variations in surface gravity affect line strengths (and abundances) by as much as 10 per cent. We also show indicative spectral types in the figure. These are based on the temperature-spectral type relation given by Pecaut & Mamajek (2013).[2] As empirical compilations of BP–W1 are not yet available, we use synthetic spectra to compute colours over a range of effective temperatures, and shift the zero-point to reproduce the colours of the Sun.

The plot reveals that for M- and late K dwarfs any amount of lithium left in the atmosphere will still show up at EW(Li) > 0.1 Å while only high abundances can be easily detected in G dwarfs. The change of abundance in late K and early M stars affects EW(Li) to a much greater extent than in early K dwarfs. In addition to this, the depletion rate depends on stellar mass and occurs on shorter time-scales for early M than K dwarfs (Mentuch et al. 2008; Soderblom et al. 2014). Assuming the initial absolute abundance of 3.26 (Asplund et al. 2009), the Baraffe et al. (2015) models of lithium depletion combined with the Pavlenko & Magazzu (1996) curves of growth were used to derive lithium isochrones as indicated in Fig. 6
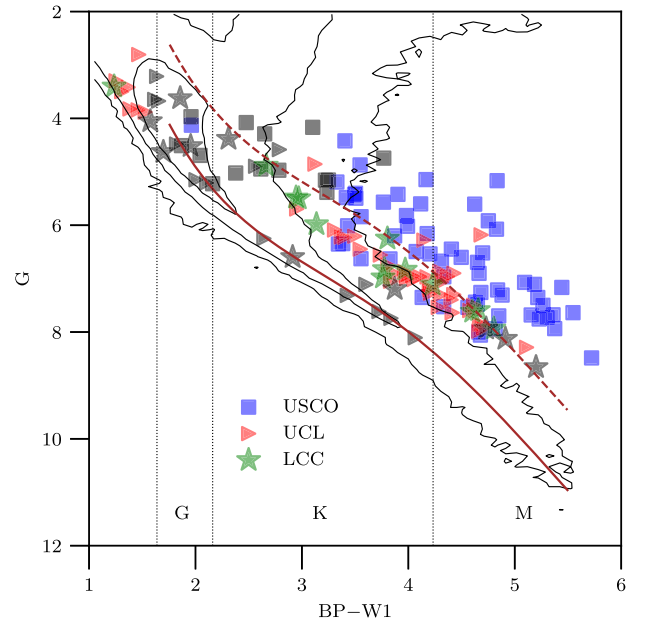
**Figure 7.** Bonafide and new candidate members of the Scorpius–Centaurus association with measurable lithium line. Candidates with questionable membership due to their EW(Li) (and in some cases their evolutionary stage) not corresponding to the expected values for their colour and age are shown in black.

with the blue solid lines. All M and late K dwarfs with detectable lithium are younger than 15–20 Myr (30 Myr, respectively) and thus still in their pre-main sequence phases.

The overlap of our GALAH sample and the known and new candidate moving group members (378 stars) found by the Banyan Σ code (G18) have been colour-coded with their age (their membership is discussed in the next subsection). Stars with similar colour and EW(Li) and hence similar nominal age are rather scattered in the plot, well beyond the internal measurement error of this work. According to Soderblom (2010), much of the scatter for the coolest stars is real. Soderblom et al. (1993) and recently Bouvier et al. (2018) report on the correlation between lithium and rotation in the Pleiades, but the origin of the scatter is not yet confirmed. Additionally, binary stars have not been treated separately in this work, and spectra of some stars (especially pre-main sequence, e.g. T Tauri objects) might be affected by veiling that causes lines to appear shallower.

### 4.1 New candidate members of young associations

The crossmatch between the G18 bonafide members and the entire GALAH sample using stellar designations revealed 91 stars that are known members of the young associations. However, since GALAH provides radial velocities (Buder et al. 2018; Zwitter et al. 2018) and completes the 6D positional and kinematic information, 305 new candidate members have been found with the Banyan Σ code (G18) using parallaxes and proper motions from *Gaia*. Only stars with radial velocity uncertainties smaller than 1 km s$^{-1}$ were considered. Note that M dwarfs from the manually selected subsample of 3519 spectra (Section 2) have not been included in the Banyan Σ membership test due to their relatively large uncertainties in radial velocities.

Membership probabilities are always more than 0.5; in fact, most of them are practically 1. However, it is clear that for individual stars,
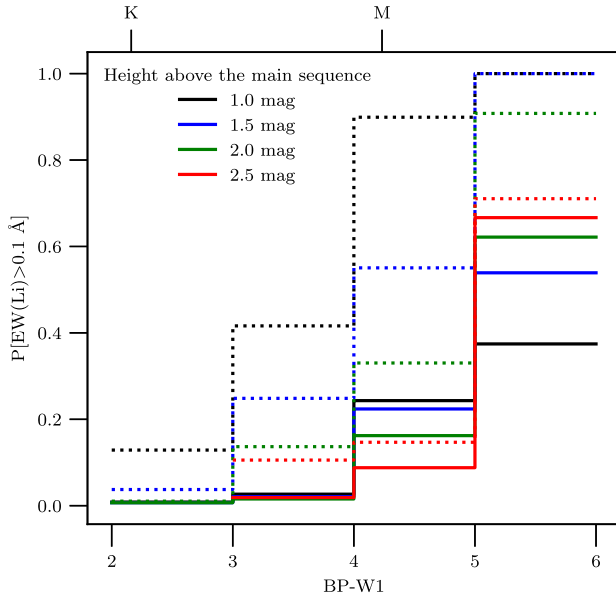
**Figure 8.** Probability that a star is young (EW(Li) > 0.1 Å) if above the main sequence (solid lines). Dotted lines represent fraction of all young stars in the sample within the colour range residing above a selected height from the main sequence. Selection of young stars above the main sequence is most effective for BP–W1 > 5 as contamination is the lowest and nearly all young stars can be recovered.

a high membership probability of an association from Banyan Σ does not in fact mean that the star is likely to be young. For example, only 41 per cent Octans (OCT) candidates and 19 per cent candidates of the Taurus–Auriga [TAU; 1–2 Myr in G18, but Kraus et al. (2017) argue that it is host to a distributed older population with 10–20 Myr; we assume that its age is 20 Myr] show lithium strength equal or greater than expected at their age (Fig. 6). In the entire sample of candidates, only 150 reside above their expected isochrone. Because a more detailed analysis of the membership is beyond the scope of this paper, we merely summarize results from the Banyan Σ code (Table 2) and provide a full candidate list (Table 3).

Half of the new candidates (154) are related to the Scorpius–Centaurus association. Fig. 7 shows a colour–magnitude diagram of the candidate stars for each of the three subgroups (Upper Scorpius – USCO, Upper Centaurus-Lupus – UCL and Lower Centaurus-Crux – LCC). Although most of them show EW(Li) above the detection threshold, the inconsistency with the expected lithium depletion at their age in some cases makes their membership questionable. 123 stars though have EW(Li) above the expected values.

## 4.2 Young stars from absolute magnitudes

High EW(Li) are found in young cool stars. At the same time, such M stars reside above the main sequence. This section addresses the possibility of identifying young stars from the broad-band photometry and the *Gaia* parallaxes alone using lithium as a test of the procedure. To better understand the relation between lithium strength and the location of young stars on the colour–magnitude diagram, the main sequence itself must first be parameterized. A polynomial of the 5th order was fitted to the median values of the colour in each of the bins in the absolute G magnitude (bin size 0.2 mag in G) for $G > 4$ and BP–W1 < 6. Effectively, this

**Table 2.** Summary of bonafide (G18) and new Banyan Σ candidate members in GALAH. Their EW(Li) was compared with the expected values for their age; 'EW(Li) > expected' lists number of stars with EW(Li) equal or higher than expected values. No info is provided for groups above 100 Myr or those with stars outside the isochrone interpolation colour range.

| Name | Bonafide | New candidates | EW(Li) > expected |
|------|----------|----------------|-------------------|
| USCO | 14 | 65 | 55 |
| UCL | 2 | 65 | 51 |
| LCC | 3 | 25 | 16 |
| PLE | 31 | 36 | / |
| HYA | 34 | 25 | / |
| OCT | 0 | 41 | 17 |
| TAU | 4 | 21 | 4 |
| ABDMG | 0 | 8 | / |
| IC2602 | 1 | 6 | 0 |
| BPMG | 0 | 3 | 3 |
| CARN | 0 | 3 | / |
| CAR | 0 | 2 | 1 |
| THA | 0 | 2 | 1 |
| TWA | 0 | 1 | 0 |
| PL8 | 0 | 1 | 1 |
| UCRA | 0 | 1 | 1 |
| EPSC | 1 | 0 | 0 |
| ROPH | 1 | 0 | 0 |
| Total | 91 | 305 | 150 |

polynomial is a curve connecting the densest parts of the main sequence. The fit was performed for all filter combinations among (BP, G, RP, J, H, $K_s$, W1, W2). BP, G, and RP are obtained from the *Gaia* DR2 photometric catalogue (Evans et al. 2018), J, H, and $K_s$ are 2MASS magnitudes (Skrutskie et al. 2006) while W1 and W2 are from the WISE catalogue (Cutri & et al. 2014).

The BP–W1 colour turned out to have the least dispersion around the main sequence in the G magnitude:

$$G = 4.717 \cdot 10^{-3} \, c^5 - 0.149 \, c^4 + 1.662 \, c^3$$
$$- 8.374 \, c^2 + 20.728 \, c - 14.129, \qquad (2)$$

where $c$ is BP–W1.

If the criterion for stellar youth is EW(Li) > 0.1 Å, then the probability that a star at a selected height above the main sequence is young, can be estimated. Ideally, we would like to select all young stars of a certain spectral type and keep contamination level as small as possible. This is easiest to achieve for M dwarfs with BP–W1 > 5 (Fig. 8) as their approach towards the main sequence is the slowest. Binary levels increase significantly below BP–W1 = 5 while a fraction of young stars is still recovered. If selecting stars with BP–W1 > 5 and 1.5 mag or more above the main sequence, all young objects are included, but 50 per cent of all selected stars are lithium-weak. In other words, selection of young stars above the main sequence is highly effective for M dwarfs, moderately effective for K dwarfs and ineffective for G dwarfs.

Apart from reddening, the spread of the main sequence in luminosity (absolute magnitude) is caused by different metallicities and stellar multiplicity. Binaries are 0.75 mag or less above the main sequence. Binaries have not been treated separately, but the presence of lithium still means that the system is young.

## 5 CONCLUSIONS

This work addresses the search for nearby young stars using the lithium 6708 Å absorption line. A simple but robust, model-free

**Table 3.** List of candidate members of known moving groups based on the Banyan Σ (Gagné et al. 2018) algorithms. Bonafide stars are confirmed members from their paper. Best hypothesis and probability $p$ are the Banyan Σ results, and Galactic spatial and velocity coordinates $XYZ$ and $UVW$, respectively, are taken from the same code. Where applicable, EW(Li) > expected gives information on whether lithium is at least as strong as expected for stellar age. Full version is available online.

| Designation Gaia DR2 | EW(Li) Å | $\sigma$(EW(Li))$_-$ Å | $\sigma$(EW(Li))$_+$ Å | Bonafide | Best hypothesis | $p$ | EW(Li) > expected | X (pc) | Y (pc) | Z (pc) | U (km s$^{-1}$) | V (km s$^{-1}$) | W (km s$^{-1}$) |
|---|---|---|---|---|---|---|---|---|---|---|---|---|---|
| 6081729701812391168 | 0.420 | 0.009 | 0.013 | NULL | LCC | 0.9987 | True | 70.75 ± 0.47 | −92.9 ± 0.62 | 26.52 ± 0.18 | −6.90 ± 0.12 | −20.39 ± 0.12 | −4.99 ± 0.09 |
| 6145079232247364096 | 0.089 | 0.003 | 0.015 | NULL | LCC | 0.9530 | False | 52.28 ± 0.23 | −103.46 ± 0.46 | 41.86 ± 0.19 | −8.75 ± 0.10 | −20.15 ± 0.14 | −5.56 ± 0.06 |
| 6045116961039667328 | 0.251 | 0.005 | 0.008 | NULL | UCL | 0.9922 | False | 127.75 ± 0.83 | −21.28 ± 0.14 | 34.11 ± 0.22 | −2.27 ± 0.45 | −20.36 ± 0.13 | −3.46 ± 0.16 |
| 3314109916508904064 | 0.087 | 0.002 | 0.002 | Hyades | HYA | 0.9996 | N/A | −43.53 ± 0.10 | 0.62 ± 0.001 | −16.79 ± 0.04 | −42.14 ± 0.08 | −19.50 ± 0.04 | −0.42 ± 0.05 |
| 4791781625391720 | 0.018 | 0.013 | 0.013 | NULL | HYA | 0.9986 | N/A | −49.48 ± 0.19 | 2.40 ± 0.01 | −18.69 ± 0.07 | −43.15 ± 0.25 | −19.25 ± 0.07 | −0.72 ± 0.12 |
| 6497973274968016 | 0.154 | 0.004 | 0.004 | Pleiades | PLE | 0.9999 | N/A | −119.35 ± 0.70 | 27.48 ± 0.16 | −54.47 ± 0.32 | −6.90 ± 0.16 | −27.47 ± 0.14 | −14.29 ± 0.15 |

approach is used to determine equivalent widths EW(Li) with a data-driven method for G, K, and early M dwarfs. The selection of lithium-weak templates for each candidate spectrum is based on the 27 spectral regions (Figs 1 and 2). The EW(Li) is given as a median value of equivalent widths within 6707.78 ± 0.75 Å for each of the (on average) 15 residual spectra. Median spectra for selected colour bins demonstrate increasing strength of Li with EW(Li) (Fig. 3). Typical uncertainties of EW(Li) are ±0.006 Å (±0.015 Å for M dwarfs) and are comparable with uncertainties originating solely from fundamental noise and template mismatch. Most EW(Li) fall below 0.7 Å with individual cases up to 1 Å (Fig. 4).

With this procedure, 3147 stars have been found to have measurable lithium: 1408 G and 892 K0-K5 (EW(Li) > 0.1 Å), 335 K5-K9 (EW(Li) > 0.07 Å) and 512 M0–M4 dwarfs (EW(Li) > 0.05 Å) (Table 1). Most of the latter reside above the main sequence (Fig. 5). While it is still possible to measure lithium in M dwarfs with a small fraction of initial lithium left, a detectable EW(Li) in early K stars traces only lithium-rich objects (Fig. 6).

A combination of the lithium information and 6D stellar kinematics (using GALAH radial velocities) is used to investigate the new candidate membership of the known associations (Table 3). In particular, we find 305 new candidates, 123 of which belong to the Scorpius–Centaurus association (Fig. 7), 36 are Pleiades cluster and 25 Hyades cluster candidate members.

Information on the strength of the lithium line for the majority of the nearby dwarfs in a volume-limited sample is not yet available, but photometric data combined with *Gaia* parallaxes to search for objects residing above the main sequence is the most straightforward approach towards a list of all candidate nearby young stars. Fig. 8 investigates contamination levels and completeness for samples of stars with increasing distance from the main sequence. Contamination levels increase significantly (almost 80 per cent) below BP–$W1$ = 5 (M2 dwarfs) while a fraction of young stars are still recovered. To confirm young photometric candidates and search for adolescent stars that have just settled on the ZAMS, large spectroscopic surveys observing lithium and youth-sensitive regions in all nearby dwarfs are essential in the future [e.g. the FunnelWeb survey (Rains et al., in preparation) and SDSS-V Kollmeier et al. 2017].

## ACKNOWLEDGEMENTS

of Education and Research. This research made use of Astropy, a community-developed core Python package for Astronomy (Astropy Collaboration 2013, 2018).

## REFERENCES

Asplund M., Grevesse N., Sauval A. J., Scott P., 2009, ARA&A, 47, 481

Astropy Collaboration et al. Astropy Collaboration, 2013, A&A, 558, A33

Astropy Collaboration et al., 2018, AJ, 156, 123

Baines E. K. et al., 2012, ApJ, 761, 57

Baraffe I., Homeier D., Allard F., Chabrier G., 2015, A&A, 577, A42

Barden S. C. et al., 2010, in McLean I. S., Ramsay S. K., Takami H., eds, Proc. SPIE Conf. Ser. Vol. 7735, Ground-based and Airborne Instrumentation for Astronomy III. SPIE, Bellingham, p. 773509

Batalha N. M. et al., 2013, ApJS, 204, 24

Boisse I. et al., 2012, A&A, 545, A55

Borucki W. J. et al., 2010, Science, 327, 977

Bouvier J. et al., 2018, A&A, 613, A63

Buder S., et al., 2018, MNRAS, 478, 4513

Cirasuolo M., 2016, in Skillen I., Balcells M., Trager S., eds, ASP Conf. Ser. Vol. 507, Multi-Object Spectroscopy in the Next Decade: Big Questions, Large Surveys, and Wide Fields. Astron. Soc. Pac., San Francisco, p. 109

Contro B., Horner J., Wittenmyer R. A., Marshall J. P., Hinse T. C., 2016, MNRAS, 463, 191

de Jong R. S. et al., 2012, McLean I. S., Ramsay S. K., Takami H., Proc. SPIE Conf. Ser. Vol. 8446, in Ground-based and Airborne Instrumentation for Astronomy IV. SPIE, Bellingham, p. 84460T

de Laverny P., Recio-Blanco A., Worley C. C., Plez B., 2012, A&A, 544, A126

De Silva G. M., Freeman K. C., Bland-Hawthorn J., Asplund M., Bessell M. S., 2007, AJ, 133, 694

De Silva G. M. et al., 2015, MNRAS, 449, 2604

Driver S. P., Davies L. J., Meyer M., Power C., Robotham A. S. G., Baldry I. K., Liske J., Norberg P., 2016, in Napolitano N. R., Longo G., Marconi M., Paolillo M., Iodice E., eds, Astron. Space Sci. Proc. Vol. 42, The Universe of Digital Sky Surveys. Springer-Verlag, Berlin, p. 205

Evans D. W. et al., 2018, A&A, 616, 21

Gagné J., Faherty J. K., 2018, ApJ, 862, 12

Gagné J. et al., 2018, ApJ, 856, 23

Gaia Collaboration et al., 2018, A&A, 616, A1

Gilmore G. et al., 2012, The Messenger, 147, 25

Ginsburg A. et al., 2018, astropy/astroquery: v0.3.7 release. https://doi.org/10.5281/zenodo.1160627

Goździewski K., Migaszewski C., 2014, MNRAS, 440, 3140

Götberg Y., Davies M. B., Mustill A. J., Johansen A., Church R. P., 2016, A&A, 592, A147

Jeffries R. D., 2014, in Lebreton Y., Valls-Gabaud D., Charbonnel C., eds, EAS Publications Series Vol. 65, The Ages of Stars. Cambridge Univ. Press, Cambridge, p. 289

Kollmeier J. A. et al., 2017, preprint (arXiv:1711.03234)

Konopacky Q. M., Marois C., Macintosh B. A., Galicher R., Barman T. S., Metchev S. A., Zuckerman B., 2016, AJ, 152, 28

Kos J. et al., 2017, MNRAS, 464, 1259

Kraus A. L., Herczeg G. J., Rizzuto A. C., Mann A. W., Slesnick C. L., Carpenter J. M., Hillenbrand L. A., Mamajek E. E., 2017, ApJ, 838, 150

Kunder A. et al., 2017, AJ, 153, 75

Lind K., Asplund M., Barklem P. S., 2009, A&A, 503, 541

Luo A. L. et al., 2015, Res. Astron. Astrophys., 15, 1095

Majewski S. R. et al., 2017, AJ, 154, 94

Mamajek E. E., Hillenbrand L. A., 2008, ApJ, 687, 1264

Marcy G. W., Butler R. P., Fischer D. A., Laughlin G., Vogt S. S., Henry G. W., Pourbaix D., 2002, ApJ, 581, 1375

Marois C., Macintosh B., Barman T., Zuckerman B., Song I., Patience J., Lafrenière D., Doyon R., 2008, Science, 322, 1348

Marois C., Zuckerman B., Konopacky Q. M., Macintosh B., Barman T., 2010, Nature, 468, 1080

Marshall J., Horner J., Carter A., 2010, Int. J. Astrobiol., 9, 259

Martell S. L. et al., 2017, MNRAS, 465, 3203

Mentuch E., Brandeker A., van Kerkwijk M. H., Jayawardhana R., Hauschildt P. H., 2008, ApJ, 689, 1127

Mullally F. et al., 2015, ApJS, 217, 31

Noyes R. W., Hartmann L. W., Baliunas S. L., Duncan D. K., Vaughan A. H., 1984, ApJ, 279, 763

Pavlenko Y. V., Magazzu A., 1996, A&A, 311, 961

Pecaut M. J., Mamajek E. E., 2013, ApJS, 208, 9

Pedregosa F. et al., 2011, J. Machine Learn. Res., 12, 2825

Perryman M., Hartman J., Bakos G. Á., Lindegren L., 2014, ApJ, 797, 14

Perryman M. A. C. et al., 1998, A&A, 331, 81

Ricker G. R. et al., 2015, J. Astron. Telescopes Instrum. Syst., 1, 014003

Rizzuto A. C., Mann A. W., Vanderburg A., Kraus A. L., Covey K. R., 2017, AJ, 154, 224

Sartoretti P. et al., 2018, A&A, 616, A6

Schmidt S. J., Hawley S. L., West A. A., Bochanski J. J., Davenport J. R. A., Ge J., Schneider D. P., 2015, AJ, 149, 158

Sharma S. et al., 2018, MNRAS, 473, 2004

Skrutskie M. F. et al., 2006, AJ, 131, 1163

Snellen I., Brown A., 2018, Nature Astron., 2, 883

Soderblom D. R., 2010, ARA&A, 48, 581

Soderblom D. R., Hillenbrand L. A., Jeffries R. D., Mamajek E. E., Naylor T., 2014, in Beuther H., Klessen R. S., Dullemond C. P., Henning T., eds, Protostars and Planets VI. Univ. Arizona Press, Tucson, p. 219

Soderblom D. R., Jones B. F., Balachandran S., Stauffer J. R., Duncan D. K., Fedele S. B., Hudon J. D., 1993, AJ, 106, 1059

Traven G. et al., 2017, ApJS, 228, 24

Wertz O., Absil O., Gómez González C. A., Milli J., Girard J. H., Mawet D., Pueyo L., 2017, A&A, 598, A83

West A. A., Hawley S. L., Bochanski J. J., Covey K. R., Reid I. N., Dhital S., Hilton E. J., Masuda M., 2008, AJ, 135, 785

Wittenmyer R. A. et al., 2014, ApJ, 783, 103

Wittenmyer R. A. et al., 2016, ApJ, 819, 28

Wittenmyer R. A. et al., 2018, AJ, 155, 84

Wright E. L. et al., 2010, AJ, 140, 1868

Yanny B. et al., 2009, AJ, 137, 4377

Zhao J.-K. et al., 2015, Res. Astron. Astrophys., 15, 1282

Zwitter T. et al., 2018, MNRAS, 481, 645

Žerjal M. et al., 2017, ApJ, 835, 61

## SUPPORTING INFORMATION

Supplementary data are available at *MNRAS* online.

**Table 1.** List of GALAH stars with measured lithium equivalent width.

**Table 3.** List of candidate members of known moving groups based on the Banyan Σ (Gagné et al. 2018) algorithms. Bonafide stars are confirmed members from their paper. Best hypothesis and probability *p* are the Banyan Σ results, and Galactic spatial and velocity coordinates *XYZ* and *UVW*, respectively, are taken from the same code. Where applicable, EW(Li) > expected gives information on whether lithium is at least as strong as expected for stellar age.

Please note: Oxford University Press is not responsible for the content or functionality of any supporting materials supplied by the authors. Any queries (other than missing material) should be directed to the corresponding author for the article.

This paper has been typeset from a TEX/LATEX file prepared by the author.